HHS Public Access

Author manuscript

Nat Chem Biol. Author manuscript; available in PMC 2011 September 01.

Published in final edited form as:

Nat Chem Biol. 2011 March ; 7(3): 168–173. doi:10.1038/nchembio.523.

Structural landscape of the isolated ligand binding domain of single AMPA receptors

Christy F. Landes[‡,†], **Anu Rambhadran**[*], **J. Nick Taylor**[†], **Ferandre Salatan**[†], and **Vasanthi Jayaraman**[‡,*]

[†] Department of Chemistry, MS 60, Rice University, Houston, Texas 77251-1892

[*]Center for Membrane Biology, Department of Biochemistry and Molecular Biology, Graduate School of Biomedical Sciences, University of Texas Health Science Center, Houston, Texas 77030

Abstract

α-amino-3-hydroxy-5-methyl-4-isoxazole propionate (AMPA) receptors mediate fast excitatory neurotransmission by converting chemical signals into electrical signals. Thus, it is important to understand the relationship between their chemical biology and their function. Single molecule fluorescence resonance energy transfer (smFRET) was used to examine the conformations explored by the agonist binding domain of the AMPA receptor for wild type and T686 mutant proteins. Each form of the agonist binding domain exhibited a dynamic, multi-state sequential equilibrium, which could only be identified using wavelet shrinkage, a signal processing technique that removes experimental shot-noise. These results illustrate that the extent of activation is dependent not on a rigid closed cleft, but instead on the probability that a given subunit will occupy a closed cleft conformation, which in turn is not only determined by the lowest energy state but by the range of states that the protein explores.

α-amino-3-hydroxy-5-methyl-4-isoxazole propionate (AMPA) receptors, a subtype of ionotropic glutamate receptor[1], are the primary mediators of fast excitatory neurotransmission in the central nervous system[2-3], and as such the role their chemical biology plays in memory and learning is of intense interest[4]. These receptors are composed of four subunits arranged in a dimer of dimer configuration[5-6]. Each subunit has an extracellular N-terminal domain and agonist binding domain, transmembrane segments that surrounds a central ion channel and an intracellular C-terminus[6]. Glutamate binding to an extracellular agonist binding domain (ABD) in each of the subunits leads to series of

Corresponding authors: Christy F. Landes, Department of Chemistry, MS 60, Rice University, Houston, Texas 77251-1892, Phone: 1-713-348-4232, Fax: 1-713-348-5155, cflandes@rice.edu; Vasanthi Jayaraman, Department of Biochemistry and Molecular Biology, University of Texas Health Science Center, Houston, Texas 77030, Phone: 1-713-500-6236, vasanthi.jayaraman@uth.tmc.edu.

Author Contributions: C. Landes and V. Jayaraman directed the research and wrote the manuscript. A. Rambhadran prepared and purified the protein samples and performed single molecule experiments. J. N. Taylor analyzed the single molecule data and prepared figures, F. Salatan performed single molecule experiments and analyzed data.

Competing Financial Interests Statement: I declare that the authors have no competing interests as defined by Nature Publishing Group, or other interests that might be perceived to influence the results and/or discussion reported in this article.

conformation changes that ultimately result in the formation of a cation permeable transmembrane channel in the receptor which subsequently closes (desensitizes) in the continued presence of agonist[7-9]. The allosteric mechanism by which the agonist mediates activation and desensitization remains one of the primary questions in this class of proteins.

Different mechanisms have been proposed for this allosteric mechanism. The initial X-ray structures of the ABD of the GluR2 subunit of AMPA receptors (Figure 1) showed a graded cleft closure of the bilobed agonist domain upon binding agonist of varying efficacy[7-12]. Hence it has been proposed that the extent of cleft closure is the primary coupling mechanism by which the agonist controls extent of activation[9]. Several exceptions to this correlation have been, however, recently observed. The willardiines for instance show no significant differences in the extent of cleft closure in the solution based NMR structures[13]. The L650T mutant and the T686S also show deviations from this correlation with a more closed cleft when bound to AMPA and glutamate respectively, even though these exhibit partial agonism[11,14-15]. While X-ray and ensemble FRET have provided the first insight into the structural changes in the ABD, they are limited by the fact that they provide the structure of the lowest energy state or average measurements of the state of the protein, respectively. In order to gain a complete understanding it is essential to determine the range of states that the protein explores. Here we have been able to do this by directly measuring all the configurations that the protein explores using smFRET to study the GluR2 agonist binding domain (GluR2-ABD) in the apo and glutamate bound state for the wild type protein and T686S mutant. These smFRET measurements are able to tie together the data from the previous measurements and are also able to identify the reasons for the discrepancies in the proposed mechanism.

Theoretical investigations of the ABD have shown that the T686 mutants deviate from the cleft closure hypothesis due to fact that the protein is more dynamic and explores configurations that are futile in terms of being able to mediate channel opening and these correlate well with the electrophysiological measurements on this mutant protein[16]. The data presented here provide the first experimental proof for the theoretically proposed energy landscape of the protein.

One problem hindering single-molecule fluorescence resonance energy transfer (smFRET) studies on proteins is that often, experiments yield a broad distribution of FRET values and thus possible conformations[17-20]. The first task is to determine if there are experimental parameters such as immobilization or dye-peptide interactions that introduce artificial spread to the data[21]. If this has been accomplished then a further challenge lies with the difficulty in using established methods to extract underlying states or rate constants[22-23]. These methods require the ability to make some initial assumption about either the states or rate constants, and this is only possible if the system or the data present a finite number of obvious choices. Otherwise, we are left with the simple, but physically meaningless, task of fitting a broad, featureless smFRET distribution with multiple Gaussians. Recently there has been some success at developing analytical tools that do not make assumptions about the underlying states[17,24]. In particular, we have shown that by using wavelet data processing techniques to separate shot-noise from other types of experimental noise, it is then possible to better resolve the underlying states in a smFRET sample[25-26].

It is this wavelet-based technique that makes it possible in the current work to quantify the number of states in the otherwise irresolvable smFRET distribution of the GluR2-ABD. State-finding analysis of the denoised smFRET data identifies four distinct conformations in the glutamate-bound form, which is the first experimental evidence for the type of multi-state equilibria predicted by the all atom molecular dynamics simulation[16]. Dwell time analyses provide rate constants for the interconversions and indicate that the transitions are sequential. Similar analysis of the agonist-free apo form suggests that there is an additional resolvable conformation, and that there is a shift in total equilibrium away from the closed form, as would be expected in the absence of stabilizing glutamate in the binding cleft. Finally, when glutamate is present with a protein mutant in which hydrogen bonding in the binding cleft is hindered, the resulting, floppier protein explores a broader range of both open and closed conformations.

Results

Denoising Single smFRET Trajectories

The first, and crucial, step in characterizing the conformational landscape for the GluR2-ABD proteins is to increase the resolution in an otherwise broad distribution of apparent FRET values. In our previous work, it was demonstrated that wavelet denoising algorithms can be used to accurately extract FRET states that are indistinguishable in the raw data due to shot-noise broadening[25,26]. In one example, a two-state equilibrium between 0.81 and 0.89 FRET states was presented, for which the ensemble smFRET histogram was broadened by shot-noise and the two states were irresolvable. After denoising, it was possible to accurately identify the states as well as their distributions, and to accurately calculate the rate constants for the transitions (Supplementary Results, Supplementary Figure 5). What results is a sharper FRET distribution, because up to 70% of the shot noise has been removed from the histogram.

A representative smFRET trace of a single glutamate-bound GluR2-ABD protein is shown in Figure 2A. The single donor/acceptor labeled GluR2-ABD smFRET trajectories, collected at 1 ms resolution, were binned to 10 ms for data analysis. In addition to traditional processing for background and crosstalk correction, as described previously[27-28], each trace was denoised using wavelet decomposition[25-26], by which it is possible to separate shot-noise from the underlying signal. The results of denoising smFRET for a single protein are shown in Figure 2B, wherein an original smFRET trace is overlain with its denoised counterpart. The associated denoised smFRET histogram is shown in Figure 2C.

Glutamate-Bound GluR2-ABD

Figure 3 includes a comparison between the ensemble raw and denoised smFRET data, in which it is shown that although the average of the distribution remains the same, the resolution is increased because the effects of shot-noise have been reduced. Ensemble histograms are compiled from many single molecule measurements for statistical analysis. The smFRET values over the ensemble of glutamate-bound GluR2-ABD molecules exhibit an average FRET value of 0.80, corresponding to an average inter-dye distance of 40.5 Å. As the dyes were attached to T394C and S652C (Figure 1), it is possible to compare this

distance to the T394-S652C distance determined by ensemble measurements. The average distance corresponds almost exactly to that determined in solution-phase ensemble FRET lifetime measurements, of 40.8 Å[14]. This result is expected, as it simply compares values from two different methods to compile ensemble values, but is of additional importance because it provides further evidence that our chosen immobilization and labeling scheme affects neither cleft closure nor dye photophysics.

The smFRET data compiled for individual molecules not only allow the identification of the exact nature of the broad distribution but also allow us to determine the different states and the type of transformation that occur between the states. This is achieved in the smFRET analysis of the GluR2-ABD because conformational features are revealed in the denoised data, as compared to the raw data. The large standard deviation of 0.14 for the raw ensemble smFRET values (Figure 3A) results in a broad and featureless distribution with no obvious conformations, and thus no experimental basis for state identification or dwell-time analysis. The particular analytical power of the wavelet denoising technique is made evident when the ensemble smFRET distribution for glutamate-bound GluR2-ABD molecules is prepared from denoised trajectories, as shown in Figure 3B. As was demonstrated in previous work, performing a hidden Markov analysis on denoised smFRET data increases the accuracy of the extracted state assignments and rate constants as compared to the same analysis performed on raw data by as much as 70%[25-26].

We used a hidden Markov model (HaMMy)[22] to fit the denoised ensemble trajectories to 2, 3, 4, 5, 6, and 7 conformational states. For each trial fit, the FRET efficiency values of the suggested conformational states were compared to those of the individual molecules using the smFRET histograms to evaluate the most consistent fit. The results indicated that four states, centered at apparent FRET values of 0.59 ± 5.8%, 0.72 ± 4.8%, 0.81 ± 4.2%, and 0.90 ± 3.8% were the minimum required to regenerate the observed distribution. Fitting with more than four states yielded redundant values. More detailed discussions of the ability of wavelet/HaMMy algorithms to accurately extract states from visibly irresolvable and four-state FRET distributions are included in our previous work[25-26] and Supplementary Methods/Results. This identification of four conformations from analysis of single, glutamate-bound GluR2-ABD molecules is the first experimental evidence in support of the complex free energy landscape predicted by all atom molecular dynamics simulations[16,29]. While the distances between the fluorophores are provided by the efficiencies of these states, the source of the distance changes could arise due to side chain rearrangements, changes in backbone orientation due to hydrogen bond changes etc. The precise nature of the conformational change associated with these distances changes cannot be determined from these measurements.

Although it is possible to extract rate constants from a Hidden Markov analysis, these values are input parameters used in optimizing the state identification algorithm[22-23]. To avoid this circular logic, and to provide an additional investigation of our four-state assignment, separate dwell-time analyses were performed to extract two pieces of information: transition rates and the numbers of transitions between non-adjacent states, which are shown in Figure 4 for the glutamate-bound GluR2-ABD. Rate constants were extracted by fitting the dwell-time distribution of each state-to-state transition to a single exponential decay. Depending on

the nature of the transition, this decay constant represents either the rate constant for the transition, or the sum of the forward or reverse rate constants, which can be calculated using the transition ratios[30].

The extracted rate constants are limited by the smFRET time resolution. Trajectories are collected in 1 ms time bins and binned to 10 ms for further data analysis. This implies that the fastest events that can be measured are on the order of 10 ms in lifetime. Under the experimental conditions used here, glutamate unbinding/binding occur 1-2 orders of magnitude faster than our time scale[31], and thus we can consider glutamate to be in its equilibrium bound state for the time window of our measurements. The rates extracted here can be compared to those obtained from NMR experiments that focused on similar phenomena[32-34], and found that stabilization of the agonist-bound domain occurred on time scales that are ms or longer[32]. These time scales differ greatly from those obtained by, for example, channel conductance experiments that measure channel opening and closing dynamics of full imbedded membrane proteins because they explore the dynamics after the binding of glutamate and initial cleft closure[35-36]. A more concrete analysis of the apparent conformational exchange rate constants would require a combination of increased time resolution and more data points.

The dwell-time analysis shown in Figure 4 was used to determine the presence or absence of conversions between non-adjacent states. Of almost three hundred transitions measured, 94% were observed to occur between adjacent states. Thus, our experimental evidence supports a four-state sequential equilibrium, as predicted by Lau and Roux[16]. Assigned FRET states and net transition equilibria are summarized in the Supplementary Results. A further analysis of the relative time scales and extracted rate constants was performed using a series of comparative kinetic Monte Carlo simulations[37-40]. Simulation details and figures are provided in the Supporting Information.

Apo GluR2-ABD

When the wavelet/HaMMy/dwell-time analysis was performed on the glutamate-free apo GluR2-ABD smFRET data, three results are apparent (Figure 5A). First, as expected from crystallographic[7,41] and traditional FRET[14] studies, the overall structure is more open. This is observed as a decrease in the average smFRET value for the apo GluR2-ABD data shown in Figure 5a. Next, the overall spread in the data, expressed as the standard deviation, indicates that the protein explores a broader potential landscape than the ligand-bound form. This has been predicted by simulations[16]. The last result is that a test of optimal HaMMy state identification suggests that a five-state depiction is more appropriate, as shown in Figure 5a along with the rate constants extracted from dwell-time analyses. These were found to be at 0.54 ± 7.3%, 0.65 ± 6.1%, 0.75 ± 5.2%, 0.84 ± 4.7%, and 0.94± 4.2%. 95% of transitions were observed to occur between adjacent states, further supporting a sequential equilibrium.

There are two possible explanations for the identification of 5 states. The first arises from an examination of the 1-dimensional free energy plot for the apo form presented by Lau and Roux[16]. Although the curve contains at least four inflection points that indicate local free energy minima, there are additional points where the curve flattens without actually

inflecting. Slight changes to the temperature or ionic conditions would shift the equilibrium enough to stabilize additional local minima. Additionally, the order parameters used in the theoretical examination were chosen for, among other qualities, their efficacy in extracting equilibrium distributions, as opposed to dynamics[16]. Different order parameters might lead to additional local minima that comprise conformational intermediates. Another explanation lies in the fact that the HaMMy state finding algorithm does not allow for broadened distributions about the mean state value[22]. The predicted energy landscape for the apo GluR2-ABD is considerably broader than that of glutamate bound protein[16], and so broad in the most open regions that the state-finding algorithm could approximate one broad state as two states with similarly narrow distribution.

T686S Mutant

The final protein of interest is the T686S mutant form of glutamate-bound GluR2-ABD, in which the ability to stabilize the glutamate bound form via hydrogen bonding is eliminated[15]. Indeed, as shown in Figure 5b, both the average smFRET value of 0.79 and the broad distribution of smFRET values support that the mutant form is more open overall, despite the presence of glutamate. This best fit to a five-state model, with similar explanations as discussed earlier for the apo form. The identified smFRET states were 0.39 ± 12%, 0.54 ± 8.7%, 0.68 ± 6.9%, 0.82 ± 5.7%, and 0.96 ± 4.9%. The dwell-time analysis yielded the rate constants shown in Figure 5b and Supplementary Table 3, and also provided consistent support for a sequential equilibrium in that 99% of transitions occurred between neighboring states.

GluR2-ABD Conformational Dynamics

This final point, relating to the overall rigidity of the three GluR2-ABD forms, can be illustrated and quantified. The characteristic fluctuation time scale (τ) of each form was calculated by determining the autocorrelation of each smFRET trajectory. An average autocorrelation curve for each set of data was created, and the curves were logarithmically binned and fit to an exponential decay[42], yielding a value of τ for each protein system. Further details regarding this calculation are included in Materials and Methods, but what is illustrated by such a comparison, as shown in Figure 6, is the decay of self- similarity within the sample. A longer decay time and higher amplitude correspond to a less rigid system, whereas the opposite traits indicate a more rigid system. For comparison, an smFRET autocorrelation decay for a more rigid biomolecule, the TAR DNA hairpin[43-44], is also included in Figure 6. These data provide clear evidence not only of the dynamic nature of GluR2-ABD, but also confirm the relative rigidity of each form. The glutamate-bound native protein is most rigid. In contrast, the apo and glutamate-bound T686S mutant proteins are more dynamic, with similar smFRET autocorrelation decay lifetimes that lie within the error of the calculated values.

Discussion

The average FRET efficiency and distance changes from the smFRET data are in good agreement with those obtained from our previous ensemble FRET analysis[14], providing independent confirmation for the validity of the smFRET data (Table 1). smFRET analysis

also offers the ability to compare *average* FRET (and distance) values with *most probable* FRET (and distance) values. As shown in Figure 5A, the rate constants for the equilibrium transitions in the apo form of the protein in the 0.65 ↔ 0.75 portion favors the more open state, with the overall result that the 0.65 state is the most probable conformation. This is in direct contrast to the glutamate-bound GluR2-ABD protein, in which all transitions favor the closed form, resulting in the 0.81 state being most prevalent, as shown in Figure 4.

The data also show that the most probable state can differ from the average state (Table 1). In examining the differences between the most probable states in the apo and glutamate bound forms extracted from the smFRET data, these data are comparable to those observed from the X-ray structures[7]. This correlation strengthens our analysis and more importantly addresses the discrepancy between the smaller changes previously reported based on the ensemble FRET data[14] relative to those observed in the X-ray structures[7].

The smFRET histograms also provide the overall spread in the states. This spread demonstrates that even in the glutamate bound form, the protein is not rigidly locked into one active form. Additionally, the smFRET data show that the protein in the apo form explores a broader potential landscape than the ligand-bound form. A broad distribution of smFRET values is also consistent with the broad landscape predicted by simulations[16]. What is most interesting about the breadth of states for the T686S mutant is that the closed form of the glutamate bound T686S mutant is nearly the same as that of the native glutamate-bound protein. This is consistent with the crystal structure of glutamate bound form of T686S that shows a closed cleft similar to that observed in glutamate bound form of the wild type protein[15].

However, the smFRET reveals that the mutant has a significantly broader range of distance distributions and more importantly probes states that have a more open cleft than that of the glutamate bound form of the wild type protein GluR2-ABD. These results suggest that the dynamics of the protein and the complete landscape that the protein probes plays a critical role in translating conformational changes to efficacy. In addition to efficacy, it has been demonstrated that the T686 mutants have the effect of increasing the recovery from desensitization [15]. Thus, it is likely that there must be a functional advantage to a less-rigid cleft in terms of neurotransmitter exchange, and what results is a trade-off between sensitivity and recovery. Also, simulations suggested that although the overall ligand-bound closed form is destabilized in the T686S mutant relative to the native protein, the mutation also decreases steric hindrance in the closure step[16]. The resulting structure is less rigid, and would be able to explore a wider range of both open and closed conformations, as is observed in the current work.

In conclusion, we have applied an advanced signal processing technique, wavelet denoising, to smFRET analysis of GluR2-ABD in order to determine that the glutamate-bound form is not a rigid, locked conformation, but instead is comprised of sequential equilibria among multiple conformations. Also, rate constants were extracted for the inter-conversions. Additionally, comparative analysis of the apo form and T686S mutant allowed us to hypothesize that there is an optimal protein flexibility that informs the functions of the apparently disparate processes of activation and desensitization. More generally, the results

illustrate that activation is dependent not on a rigid closed cleft, but instead on the probability that a given subunit will occupy a closed cleft conformation, which in turn is not only determined by the lowest energy state but by the range of states that the protein explores.

Methods

Expression and Labeling of GluR2-ABD

The GluR2 -ABD plasmid was provided by Dr Eric Gouaux (Oregon Health and Science University, Portland, OR). S652C, T394C and T686S mutations were introduced using Quick Change Site- Directed Mutagenesis Kit (Stratagene). GluR2-ABD wild type protein and T686S mutant protein (with T394C and S652C) were expressed and purified as previously described[14]. In brief, the wild type and mutant protein were expressed in *Escherichia Coli* Origami–B (DE3) cells and the Histidine tag containing proteins were subjected to purification using Ni-NTA Hi Trap column (GE Healthcare). 0.1-0.5μM protein in phosphate buffer with 1mM glutamate was used for labeling. Thiol- reactive maleimide derivatives of Alexa 555 and 647 (Invitrogen) served as donor and acceptor probes. The Alexa fluorophores are directly linked to the thiol group of the cysteines in the proteins and no additional linkers are present between the fluorophores and the protein. Unreacted excess dyes were removed by dialyzing extensively in either phosphate buffer only for Apo experiments or in phosphate buffer containing 10mM glutamate for glutamate bound single molecule experiments. Preparation of samples for the single molecule experiments were performed as described by Hanson et al.[45].

Immobilizing and Protecting GluR2-ABD

Glass slides were plasma cleaned to remove impurities from the surface. Vectabond (Vector Labs), a proprietary aminosilane, was used to amine functionalize the surface. The amine group of the Vectabond reacted with the NHS ester group of O-[2-(N-Succinimidyloxycarbonyl)-ethyl]-O'-methylpolyethylene glycol 5000 (NHS-PEG-5000 – Fluka)) and NHS-PEG-5000-Biotin (biotin-PEG – NOF Corporation). A sample chamber was assembled by placing a coverslip with two ports on top of the biotin-PEG glass slide[43,46]. The two ports were used as inlet and outlet ports for the flow system. The GluR2-ABD was attached to a biotin-conjugated anti-histidine monoclonal antibody (biotin-Anti-His Ab). The biotin-PEG slide was incubated with streptavidin (SA) solution. The SA served as the linker between the biotin-PEG slide and the biotin-Anti-His Ab – GluR2-ABD.

An oxygen scavenging flow solution was prepared by following an established protocol[27]. The flow solution was composed of 3% (wt/vol) β-D-(+)-glucose (Sigma), 0.1 mg of glucose oxidase (Roche Applied Science) per ml of solution, 0.02 mg of catalase (Roche Applied Science) per ml of solution, 2 mM $MgCl_2$, and saturated solution of Trolox powder (6-hydroxy-2,5,7,8-tetramethylchroman-2-carboxylic acid; Fluka). The Trolox powder was dissolved in PBS, then subsequently filtered[47-48]. The final flow solutions contained 10 mM glutamate in phosphate buffered saline solution in the case of the glutamate-bound experiments.

FRET Instrumentation

A diagram of our scanning confocal smFRET instrumentation is shown in the Supplementary Methods. The sample chamber with flowing oxygen scavenging solution sat on top of a closed-loop x-y-z piezo stage (P-517.3CL; Physik Instrumente) with 100 × 100 × 20 μm travel range and 1-nm specificity (SPM 1000; RHK Technology). The sample was excited using 532-nm solid state laser light (Verdi; Coherent). The power of the laser light was controlled as necessary using neutral density filters. The excitation light has a Gaussian beam profile at the sample. This was achieved by expanding the excitation light to overfill the back aperture of a FLUAR 100× 1.3 NA oil immersion microscope objective (Carl Zeiss, GmBH). The expansion resulted in a $1/e^2$ beam radius of ∼250 nm and height of ∼1 μm.

Fluorescence was collected and refocused by the same objective and was separated from the excitation light by using a dichroic mirror (z532rdc, Chroma Technology). The S/N ratio was further improved by additional emission filters (NHPF-532.0; Kaiser Optical; and ET585, Chroma Technology). The signal was refocused and passed through a second dichroic mirror (640-nm high-pass filter) to separate the donor emission from the acceptor emission. The donor and the acceptor fluorescence signals were collected by two corresponding avalanche photodiode detectors (SPCM-AQR-15; Perkin-Elmer).

Data Collection and Analysis

The molecules were excited by green laser light (532 nm). The emission intensity trajectories were collected at a 1-ms resolution and later binned up to 10 ms to enhance the S/N ratio. The fluorescence signals of the donor (I_D) and the acceptor (I_A) were collected until the fluorophores were photobleached. The apparent FRET efficiency (E_A) was calculated using the background- and crosstalk-corrected intensities by the following equation:

$$E_A = \left(\frac{I_A}{I_A + I_D} \right) \quad (1)$$

The distance between the two fluorophores was calculated with the following equation:

$$E_A = \left(1 + \left(\frac{R}{R_0} \right)^6 \right)^{-1} \quad (2)$$

where: R = is the inter-dye distance, and R_0 = is the Förster radius, which, for the Alexa555-Alexa647 pair, is approximately 5.1 nm (Molecular Probes).

Because the cleft closure is floppy in solution, the molecule is in equilibrium between multiple conformations. Therefore, it is important to determine the dwell time of the molecule in one conformation. This was done by executing an autocorrelation analysis on the FRET efficiency of each molecule, then taking the average of the autocorrelation values

to produce an ensemble autocorrelation, which is presented and analyzed with logarithmic binning to avoid over-fitting at long lag times.

$$G(\tau)=\frac{\langle \delta F(t)_{*}\ \delta F(t+\tau)\rangle}{\langle F(t)\rangle^{2}} \quad (3)$$

$$\delta F(t)=F(t)-\langle F(t)\rangle \quad (4)$$

Here, G(τ) is the calculated autocorrelation function, F(t) is the original FRET trajectory, and τ is the lag time that expresses the time shift between the original signal and the signal after the time shift. The resultant autocorrelation decays were fit with single exponential functions.

Details about the wavelet denoising technique, dwell-time analysis, and rate constant extraction can be found our earlier work[25-26] and in the Supplementary Results. All data analysis was performed with programs written in house using MATLAB (R2008b, The Mathworks, Natick, MA), with the exception of the hidden Markov state-finding analysis, which was performed with a program made available by the Taekjip Ha group at the University of Illinois at Urbana-Champaign[22].

Supplementary Material

Refer to Web version on PubMed Central for supplementary material.

Acknowledgments

C. F. Landes thanks the Norman Hackerman Welch Young Investigator Program at Rice University. Acknowledgment is made to the Donors of the American Chemical Society Petroleum Research Fund for partial support of this research (to C.F.L). This work was supported by National Institutes of Heal th Grant R01GM073102 (to V. J) and American Heart Association Grant 0855081F (VJ). The authors also thank H. Yang and R. Goldsmith for helpful suggestions.

References

1. Keinanen K, et al. A family of AMPA-selective glutamate receptors. Science (Washington, DC, United States). 1990; 249:556–560.
2. Nakanishi S, Masu M. Molecular diversity and functions of glutamate receptors. Annual review of biophysics and biomolecular structure. 1994; 23:319–348.
3. Dingledine R, Borges K, Bowie D, Traynelis SF. The glutamate receptor ion channels. Pharmacological Reviews. 1999; 51:7–61. [PubMed: 10049997]
4. Fleming JJ, England PM. AMPA receptors and synaptic plasticity: a chemist's perspective. Nature Chemical Biology. 2010; 6:89–97. [PubMed: 20081822]
5. Rosenmund C, Stern-Bach Y, Stevens CF. The tetrameric structure of a glutamate receptor channel. Science (Washington, D C). 1998; 280:1596–1599.
6. Sobolevsky AI, Rosconi MP, Gouaux E. X-ray structure, symmetry and mechanism of an AMPA-subtype glutamate receptor. Nature (London, U K). 2009; 462:745–756. [PubMed: 19946266]
7. Armstrong N, Gouaux E. Mechanisms for activation and antagonism of an AMPA-sensitive glutamate receptor: crystal structures of the GluR2 ligand binding core. Neuron. 2000; 28:165–181. [PubMed: 11086992]

8. Armstrong N, Mayer M, Gouaux E. Tuning activation of the AMPA-sensitive GluR2 ion channel by genetic adjustment of agonist-induced conformational changes. Proceedings of the National Academy of Sciences of the United States of America. 2003; 100:5736–5741. [PubMed: 12730367]
9. Gouaux E. Structure and function of AMPA receptors. Journal of Physiology (Oxford, United Kingdom). 2004; 554:249–253.
10. Armstrong N, Sun Y, Chen GQ, Gouaux E. Structure of a glutamate-receptor ligand-binding core in complex with kainate. Nature (London, United Kingdom). 1998; 395:913–917. [PubMed: 9804426]
11. Birdsey-Benson A, Gill A, Henderson LP, Madden DR. Enhanced efficacy without further cleft closure: reevaluating twist as a source of agonist efficacy in AMPA receptors. Journal of Neuroscience. 2010; 30:1463–1470. [PubMed: 20107073]
12. Ahmed AH, Wang Q, Sondermann H, Oswald RE. Structure of the S1S2 glutamate binding domain of GluR3. Proteins: Structure, Function, and Bioinformatics. 2009; 75:628–637.
13. Maltsev AS, Ahmed AH, Fenwick MK, Jane DE, Oswald RE. Mechanism of Partial Agonism at the GluR2 AMPA Receptor: Measurements of Lobe Orientation in Solution. Biochemistry. 2008; 47:10600–10610. [PubMed: 18795801]
14. Ramanoudjame G, Du M, Mankiewicz KA, Jayaraman V. Allosteric mechanism in AMPA receptors: a FRET-based investigation of conformational changes. Proc Natl Acad Sci USA. 2006; 103:10473–10478. [PubMed: 16793923]
15. Robert A, Armstrong N, Gouaux JE, Howe JR. AMPA receptor binding cleft mutations that alter affinity, efficacy, and recovery from desensitization. Journal of Neuroscience. 2005; 25:3752–3762. [PubMed: 15829627]
16. Lau AY, Roux B. The Free Energy Landscapes Governing Conformational Changes in a Glutamate Receptor Ligand-Binding Domain. Structure (Cambridge, MA, United States). 2007; 15:1203–1214.
17. Li CB, Yang H, Komatsuzaki T. Multiscale complex network of protein conformational fluctuations in single-molecule time series. Proc Natl Acad Sci USA. 2008; 105:536–541. [PubMed: 18178627]
18. Schuler B, Lipman EA, Eaton WA. Probing the free-energy surface for protein folding with single-molecule fluorescence spectroscopy. Nature. 2002; 419:743–747. [PubMed: 12384704]
19. Schuler B, Eaton WA. Protein folding studied by single-molecule FRET. Current Opinion in Structural Biology. 2008; 18:16–26. [PubMed: 18221865]
20. Flynn EM, Hanson JA, Alber T, Yang H. Dynamic Active-Site Protection by the M. tuberculosis Protein Tyrosine Phosphatase PtpB Lid Domain. Journal of the American Chemical Society. 2010; 132:4772–4780. [PubMed: 20230004]
21. Chung Hoi S, Louis John M, Eaton William A. Distinguishing between protein dynamics and dye photophysics in single-molecule FRET experiments. Biophys J. 2010; 98:696–706. [PubMed: 20159166]
22. McKinney SA, Joo C, Ha T. Analysis of single-molecule FRET trajectories using hidden Markov modeling. Biophysical Journal. 2006; 91:1941–1951. [PubMed: 16766620]
23. Talaga DS. Markov processes in single molecule fluorescence. Curr Opin Colloid Interface Sci. 2007; 12:285–296. [PubMed: 19543444]
24. Li CB, Yang H, Komatsuzaki T. New Quantification of Local Transition Heterogeneity of Multiscale Complex Networks Constructed from Single-Molecule Time Series. Journal of Physical Chemistry B. 2009; 113:14732–14741.
25. Taylor JN, Makarov DE, Landes CF. Denoising single-molecule FRET trajectories with wavelets and Bayesian inference. Biophysical Journal. 2010; 98:164–173. [PubMed: 20074517]
26. Taylor JN, Landes CF. Improved resolution of complex single-molecule FRET systems via wavelet shrinkage. Journal of Physical Chemistry B. 2011 ASAP on Web.
27. Darugar Q, Kim H, Gorelick RJ, Landes CF. Human T-Cell lympotropic virus type 1 nucleocapsid protein-induced structural changes in transactivation response DNA measured by single molecule fluorescence resonance energy transfer. J Virol. 2008; 92:12164–12171. [PubMed: 18829758]
28. Taylor JN, Darugar Q, Kourentzi K, Willson RC, Landes CF. Dynamics of an anti-VEGF aptamer: A single molecule study. Biochem Biophys Res Comm. 2008; 373:213–218. [PubMed: 18555799]

29. Mamonova T, Yonkunas MJ, Kurnikova MG. Energetics of the Cleft Closing Transition and the Role of Electrostatic Interactions in Conformational Rearrangements of the Glutamate Receptor Ligand Binding Domain. Biochemistry. 2008; 47:11077–11085. [PubMed: 18823129]
30. Benitez JJ, et al. Probing Transient Copper Chaperone-Wilson Disease Protein Interactions at the Single-Molecule Level with Nanovesicle Trapping. Journal of the American Chemical Society. 2008; 130:2446–2447.10.1021/ja7107867 [PubMed: 18247622]
31. Cheng Q, Du M, Ramanoudjame G, Jayaraman V. Evolution of glutamate interactions during binding to a glutamate receptor. Nature Chemical Biology. 2005; 1:329–332. [PubMed: 16408071]
32. Ahmed AH, Loh AP, Jane DE, Oswald RE. Dynamics of the S1S2 glutamate binding domain of GluR2 measured using 19F NMR spectroscopy. Journal of Biological Chemistry. 2007; 282:12773–12784. [PubMed: 17337449]
33. Fenwick MK, Oswald RE. On the Mechanisms of α-Amino-3-hydroxy-5-methylisoxazole-4-propionic Acid (AMPA) Receptor Binding to Glutamate and Kainate. Journal of Biological Chemistry. 2010; 285:12334–12343. [PubMed: 20110361]
34. McFeeters RL, Oswald RE. Structural mobility of the extracellular ligand-binding core of an ionotropic glutamate receptor. Analysis of NMR relaxation dynamics. Biochemistry. 2002; 41:10472–10481. [PubMed: 12173934]
35. Robert A, Howe JR. How AMPA receptor desensitization depends on receptor occupancy. Journal of Neuroscience. 2003; 23:847–858. [PubMed: 12574413]
36. Zhang W, Cho Y, Lolis E, Howe JR. Structural and single-channel results indicate that the rates of ligand binding domain closing and opening directly impact AMPA receptor gating. Journal of Neuroscience. 2008; 28:932–943. [PubMed: 18216201]
37. Makarov DE, Metiu H. A model for the kinetics of protein folding: Kinetic Monte Carlo simulations and analytical results. J Chem Phys. 2002; 116:5205–5216.
38. Fichthorn KA, Weinberg WH. Theoretical Foundations of Dynamical Monte Carlo Simulations. J Chem Phys. 1991; 95:1090–1096.
39. Metiu H, Lu YT, Zhang Z. Epitaxial Growth and the Art of Computer Simulations. Science. 1992; 255:1088–1092. [PubMed: 17817783]
40. Voter AF. Classically Exact Overlayer Dynamics: Diffusion of Rhodium Clusters on Rh(100). Phys Rev B: Condens Matt. 1986; 34:6819–6928.
41. Madden DR, Armstrong N, Svergun D, Perez J, Vachette P. Solution X-ray Scattering Evidence for Agonist- and Antagonist-induced Modulation of Cleft Closure in a Glutamate Receptor Ligand-binding Domain. Journal of Biological Chemistry. 2005; 280:23637–23642. [PubMed: 15755731]
42. Ha TJ, et al. Single-molecule fluorescence spectroscopy of enzyme conformational dynamics and cleavage mechanism. Proc Natl Acad Sci USA. 1999; 96:893–898. [PubMed: 9927664]
43. Landes CF, Zeng Y, Liu HW, Musier-Forsyth K, Barbara PF. Single-Molecule study of the Inhibition of HIV-1 transactivation response region DNA/DNA annealing by argininamide. Journal of the American Chemical Society. 2007; 129:10181–10188. [PubMed: 17658799]
44. Cosa G, et al. Secondary structure and secondary structure dynamics of DNA hairpins complexed with HIV-1 NC protein. Biophysical Journal. 2004; 87:2759–2767. [PubMed: 15454467]
45. Hanson JA, et al. Illuminating the mechanistic roles of enzyme conformational dynamics. Proc Natl Acad Sci USA. 2007; 104:18055–18060. [PubMed: 17989222]
46. Zeng Y, et al. Probing nucleation, reverse annealing, and chaperone function along the reaction path of HIV-1 single-strand transfer. Proc Natl Acad Sci USA. 2007; 104:12651–12656.10.1073/pnas.0700350104 [PubMed: 17578926]
47. Cordes T, Vogelsang J, Tinnefeld P. On the Mechanism of Trolox as Antiblinking and Antibleaching Reagent. Journal of the American Chemical Society. 2009; 131:5018–5019. [PubMed: 19301868]
48. Rasnik I, McKinney SA, Ha T. Nonblinking and long-lasting single-molecule fluorescence imaging. Nature Meth. 2006; 3:891–893.

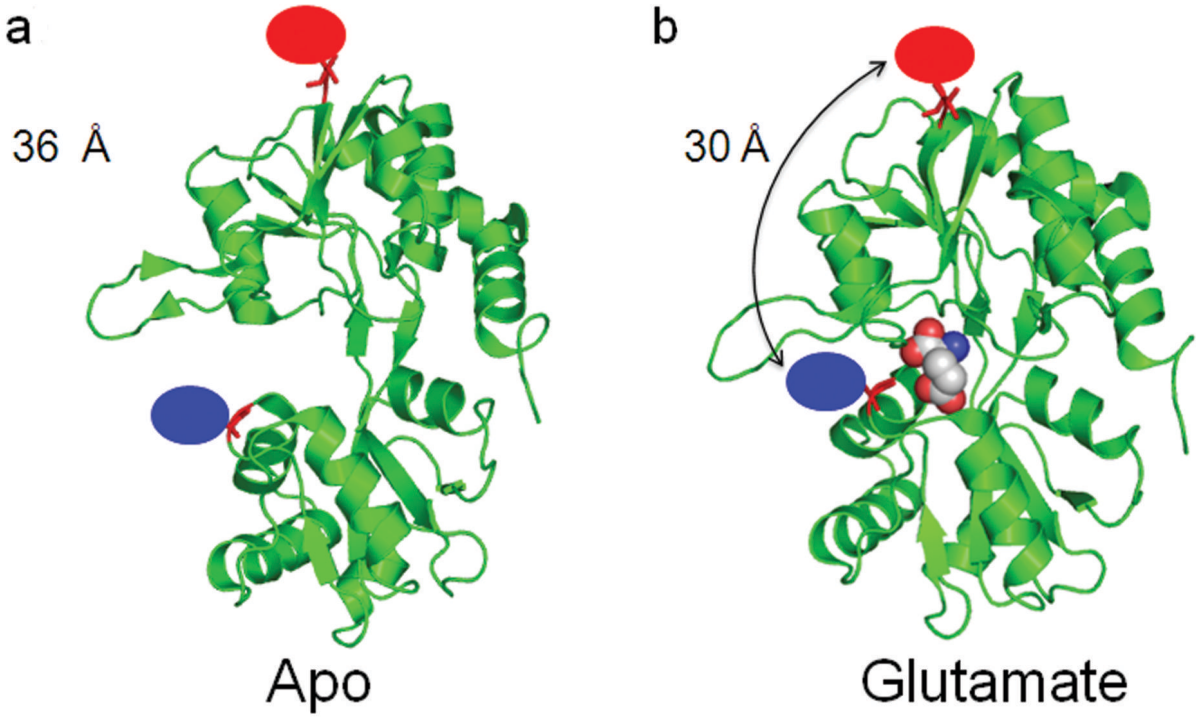

Figure 1.
Crystal structure of GluR2-ABD showing the sites labeled for the smFRET investigations and distances between the sites in the (A) apo and (B) glutamate bound form.

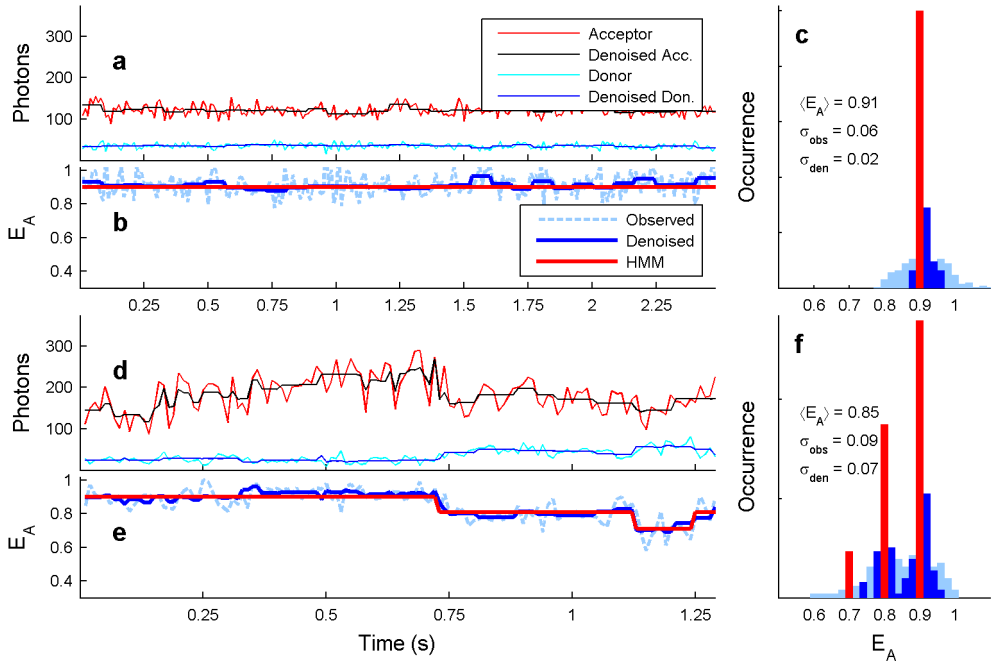

Figure 2.

Single-molecule smFRET before and after denoising. (A) Raw photon count trajectories from the acceptor and donor detectors are shown in red and cyan, respectively for a protein that exhibits a static conformation for the depicted time-duration. Denoised trajectories are also included, as indicated (and discussed in the text and Supplementary Results). (B) Calculated apparent smFRET trajectory, E_A, is shown for raw data (cyan) and denoised data (blue). Using a state-finding algorithm, HMM[22], on the denoised data, (red) accurately extracts a single state. (C) An smFRET histogram illustrates the effects of denoising on the distribution of smFRET values. Denoising is more important for proteins that are undergoing transitions to similar conformations, as is illustrated for such a protein in (D). The smFRET trajectory and (E) smFRET histogram for such a protein require the application of wavelet denoising in order to resolve the underlying states in the otherwise noisy trajectory that results from a molecule that exhibits structural dynamics.

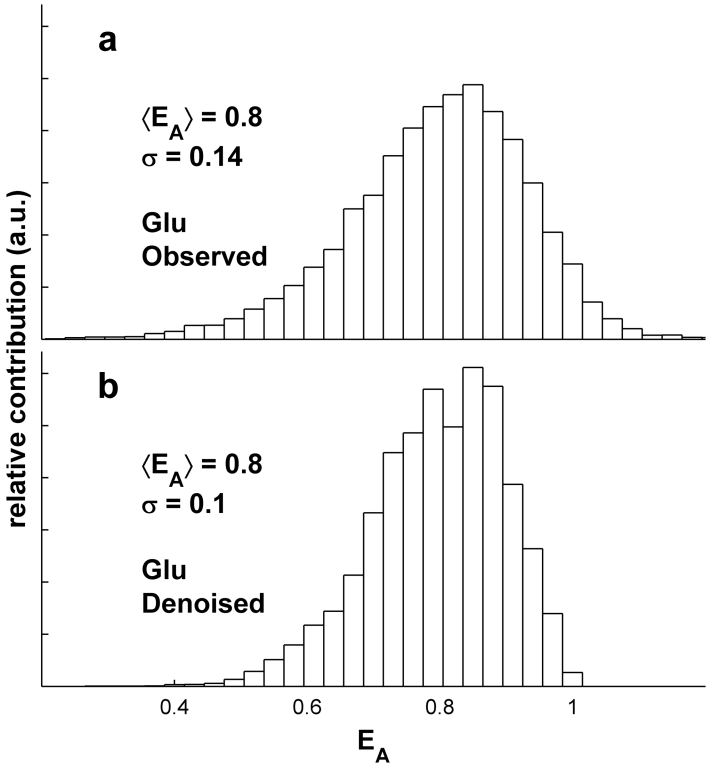

Figure 3.

(A) Distribution of FRET values from 67 glutamate-bound GluR2-ABD smFRET traces before and (B) after wavelet denoising.

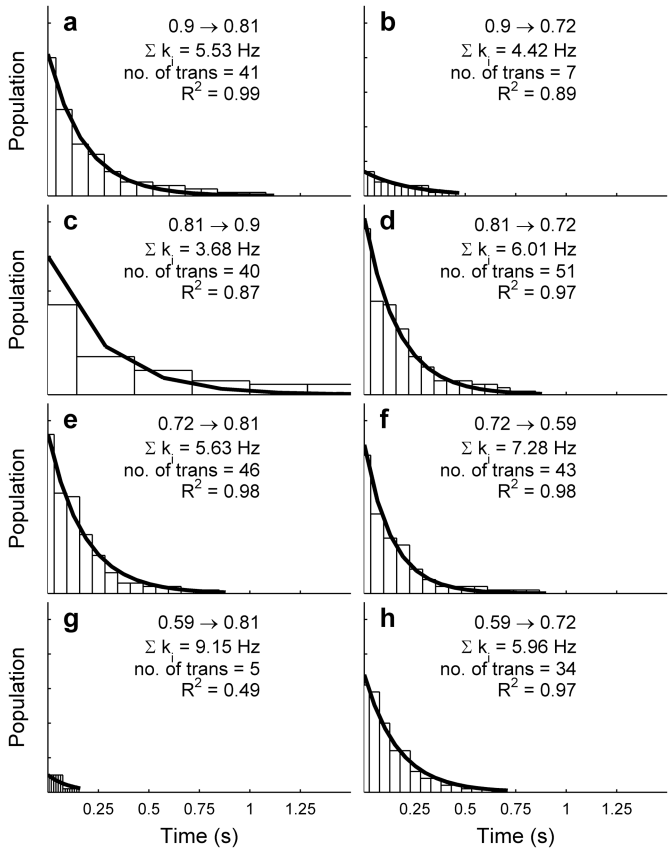

Figure 4.

Dwell-time histograms for all of the observed transitions between the four states identified from the glutamate-bound GluR2-ABD form. Each histogram was fit to a single exponential decay in order to extract transition rates. 94% of observed transitions occurred between neighboring conformations.

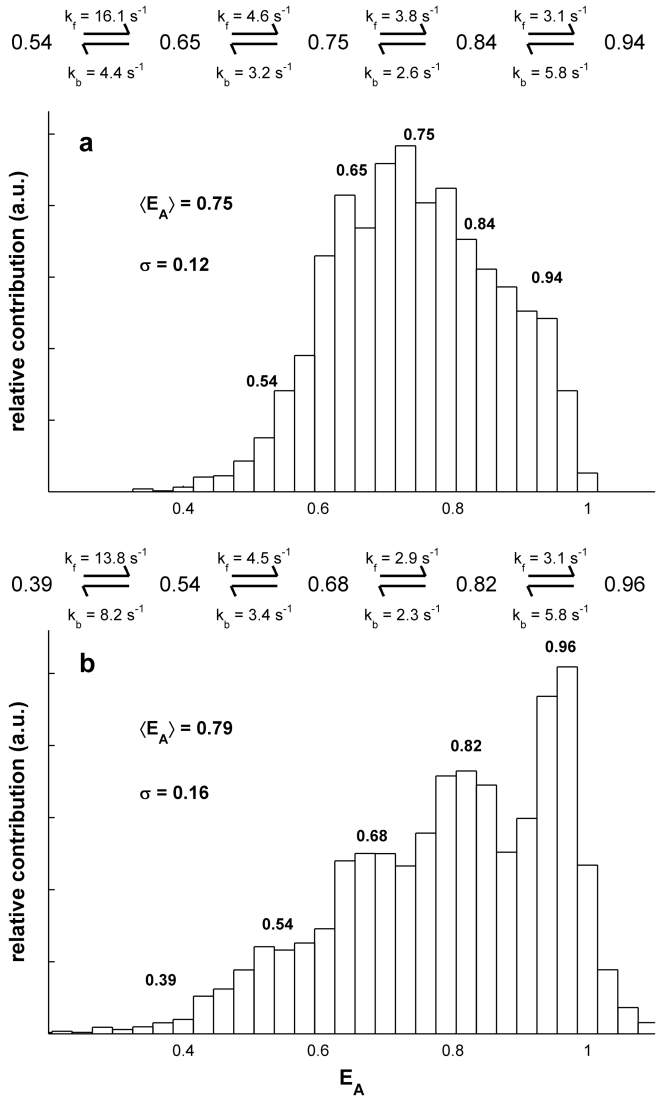

Figure 5.

(A) Denoised apo GluR2-ABD ensemble FRET histogram with the five preferred conformational states and the rate constants of the transitions for the sequential equilibrium. (B) Denoised glutamate bound form of GluR2-T686S-ABD ensemble FRET histogram. The histograms show the five preferred conformational states and the rate constants of the transitions.

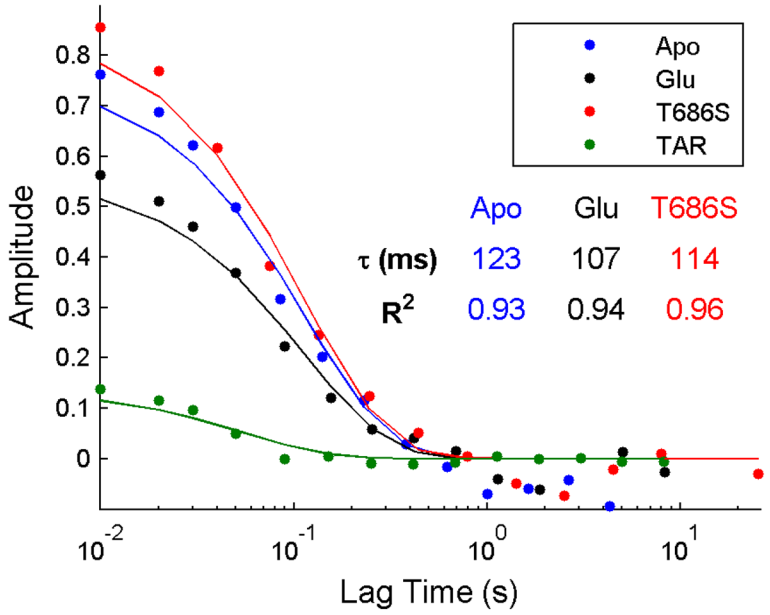

Figure 6.

The average smFRET efficiency autocorrelation as a function of lag time is compared for the three GluR2-ABD proteins measured in the current work, and compared to a similar analysis of a model rigid biomolecule, TAR DNA[43-44].

Table 1

Distances between sites 394 and 652

Method	Points of Measurement between residues 394 and 652	Apo GluR2-ABD (Å)	Glutamate bound GluR2-LBD (Å)	Difference in distance (Å)
X-Ray[7,36]	Cα to Cα	36	30	6
Ensemble FRET[14]	Average distance between Donor :Acceptor	45	41	4
smFRET	Distance between Donor :Acceptor for most probable conformation	46	40	6
smFRET	Distance between Donor :Acceptor for average conformation	43	40	3